This article has been accepted for publication in a future issue of this journal, but has not been fully edited. Content may change prior to final publication. Citation information: DOI 10.1109/TIA.2021.3117926, IEEE Transactions on Industry Applications

Multi-Period Restoration Model for Integrated Power-Hydrogen Systems Considering Transportation States

Zekai Wang, *Student Member, IEEE*, Tao Ding, *Senior Member, IEEE*, Wenhao Jia, *Student Member, IEEE*, Chenggang Mu, *Student Member, IEEE*, Can Huang, *Senior Member, IEEE*, João P. S. Catalão, *Senior Member, IEEE*

***Abstract*—This paper proposes an innovative integrated power and hydrogen distribution system (IPHDS) restoration model in response to multiple outages caused by natural disasters. During the restoration, repair crews (RCs) and mobile battery-carried vehicles (MBCVs) are considered to repair faulted lines and support critical power loads. Also, the network reconfiguration is taken into consideration in the restoration model to pick up loads. Besides, to address the different response time of hydrogen and power systems, the aerodynamic law-based dynamic hydrogen flow model is applied in the hydrogen system. The proposed model is presented as a mixed-integer linear program, which is verified on a 33-bus-48-node IPHDS with multiple outages. The present results verify the effectiveness of the proposed method.**

***Index Terms*—Resilience, integrated system restoration, repair crews, mobile battery-carried vehicles, dynamic hydrogen flow, network reconfiguration.**

I. Introduction

DUE to the global climate change, extreme weather events, e.g., hurricanes, windstorms, and typhoons, have become increasingly frequent and devastating in recent years, causing serious power outages and infrastructure damages [1]-[3]. For instance, Hurricane Sandy in 2012 brought severe damages to the power distribution systems, which led to 8.66 million customer outages [4]. Furthermore, more than 80% of power outages in the U.S. were attributed to natural disasters, and approximately 90% of them were caused by failures in distribution systems [5], [6]. Hence, it is of critical importance to enhance the resilience of power distribution systems against extreme natural disasters [7]-[17].

In [7], a robust optimization-based approach was proposed for the optimal planning of resilient distribution networks, which considered the distributed generation resource placement and grid hardening strategies. Reference [8] proposed a two-stage robust optimization framework for the optimal line hardening of the resilient distribution systems with multiple renewable resources. Based on deep reinforcement learning, a long-term planning model based on hardening strategies was proposed in [9] to improve the resilience of power distribution systems. In [10], a sequential service restoration model was formulated for distribution systems and microgrids in extreme power outage events by coordinating the distributed generators and switches. Also, [11] developed a risk-limiting load restoration approach to enhance the resilience of distribution systems with networked microgrids. In [12], a resilient model to restore critical loads from natural disasters was proposed by a microgrid formulation for distribution systems.

In addition, network reconfiguration is also an efficient method for the resilience enhancement of distribution systems [13]-[17]. Reference [13] proposed an optimal load restoration model for enhancing the distribution system resilience by utilizing the network reconfiguration and microgrid formation. Based on the topology reconfiguration and distributed generator islanding, a tri-level defender-attacker-defender framework for the resilient distribution systems was formulated in [14]. A unified two-stage reconfiguration model was established in [15] to improve the resilience of distribution networks, and the scenario decomposition method was employed to relieve the computation burden. In [16], a resilience enhancement strategy for distribution systems was presented considering islanding and dynamic reconfiguration. In [17], a novel formulation was proposed for radiality constraints to increase the flexibilities in the network reconfiguration-related optimization problems of distribution systems. Considering the network reconfiguration and distributed generators scheduling, [18] proposed a power outage management strategy for enhancing the resilience of the distribution network.

The previous papers were mainly focused on the resilience of power distribution systems, while neglecting the impact of other energy systems such as natural gas and hydrogen. In recent years, with the continuous progress in power-to-gas (P2G) technology, the electric hydrogen production (EHP) becomes feasible and economical, which can provide enormous flexibility for power grids to accommodate the intermittent power supply from renewable energy resources [19]. Therefore, the integrated power-hydrogen system (IPHS) will play a crucial role in the future energy transformation and low-carbon pathways. Besides, after a natural disaster, the power system will reach a steady-state within a few milliseconds, while the hydrogen system will change dynamically over a period of several minutes. The time scales in the power and hydrogen system

This work was supported in part by National Natural Science Foundation of China (Grant 51977166), in part by Natural Science Foundation of Shaanxi Province (2021GXLH-Z-059), and in part by the auspices of the U.S. Department of Energy by Lawrence Livermore National Laboratory under Contract DE-AC52-07NA27344 with Release Number LLNL-JRNL-946206.

Z. Wang, T. Ding, W. Jia and C. Mu are with the Department of Electrical Engineering, Xi'an Jiaotong University, Xi'an, Shaanxi, 710049, China. (email: tding15@mail.xjtu.edu.cn)

C. Huang is with Lawrence Livermore National Laboratory, Livermore, CA 94550, USA.

J. P. S. Catalão is with the Faculty of Engineering of the University of Porto (FEUP) and INESC TEC, Porto, Portugal.

are quite different from each other, indicating that the existing methodologies proposed for a resilient power system will not be suitable for an IPHS.

Several papers have studied the optimal planning and operation of the IPHS [20]-[25]. Reference [20] proposed a robust IPHS planning model that considered the power to hydrogen and heat, seasonal hydrogen storage, and N-1 reliability constraints of crucial devices. Reference [21] formulated an optimal operation framework for the IPHS with utilization of hydrogen fuel cell vehicles. In [22], a hybrid IPHS energy sharing framework was presented considering the P2G devices and plug-in hybrid electric-hydrogen vehicles. In [23], an optimal dispatch model was established for the active distribution systems considering the power-to-hydrogen-and-heat scheme. Additionally, reference [24] proposed a security constrained unit commitment model with integration of P2G devices and hydrogen gas turbines. Reference [25] proposed a joint optimization model for the power-hydrogen-heat energy systems to reduce the wind and solar power curtailment.

Although there are quite a lot of similarities between hydrogen system and natural gas system, there still exist much more difference between these two systems. On the one hand, the high safety requirements for hydrogen transmission in pipelines make it impossible to transmit hydrogen in large volumes and over long distances like natural gas. Compared with the integrated power and natural gas systems which can achieve large-scale and stable operation, the integrated power and hydrogen systems usually operate in the form of a power distribution system coupled with several small-scale hydrogen distribution systems to each other. On the other hand, the hydrogen systems and natural gas systems are operated by different agents, and the model of the integrated power and hydrogen system is also different from that of the integrated power and natural gas system. In the integrated power and natural gas system, the power system and natural gas system are managed operated by different agents, indicating that the model of integrated power and distribution system must be solved by distributed solution algorithms [26-28]. In contrast, the large-scale application of hydrogen is supposed to address the replacement of traditional fossil energy sources, and is wildly used in the power industry. The power system will become the main industry for hydrogen production and consumption in the future. Therefore, the future hydrogen system will be dependent on the operation of the power system, indicating that the model of integrated power and hydrogen system can be solved by centralized algorithms.

Furthermore, the increasing interdependency between power distribution systems and hydrogen systems will bring extraordinary challenges to the resilience of the IPHS. In addition to the electric infrastructures, the key components of hydrogen systems, such as EHPs, pipelines, storage tanks, compressors, and gas-fired units, may also get damaged by natural disasters, which makes the IPHS disaster restoration more complicated. Therefore, the existing methodologies for the power distribution system resilience [7]-[18] may no longer be applied to the resilience of the IPHS. It is necessary to mathematically characterize the new features of the IPHS, such as the transient modeling of hydrogen pipeline flow and EHP process, to set up a hybrid disaster restoration framework for the IPHS. However, all these issues have not yet been sufficiently addressed in the current publications.

Emergency response resources, such as the repair crews (RCs) and mobile power sources (MPSs), can be dispatched to the desired fields through the transportation network, providing flexibilities for the restoration strategies of the IPHS [29]-[31]. In essence, the optimal dispatch of RRCs and MPSs can be equivalent to a classical vehicle routing problem [32], [33]. Considering the hybrid dispatch of RRCs and MPSs in the transportation network, [34] proposed an optimal load restoration approach for the resilient distribution systems. In [35], a two-stage outage management strategy was suggested by co-optimizing the RRCs, topology reconfiguration, and distributed generation dispatch. Reference [36] proposed a three-stage stochastic optimization model by fully incorporating the optimal planning, pre-position, and dispatch of MPSs, thus minimizing the investment costs and improving the system resilience. In [37], a multiperiod restoration framework was proposed for the resilient distribution systems by optimally coordinating the RCs, mobile battery-carried vehicles (MBCVs), and networked microgrids formation.

In further studies, the uncertainties introduced by renewable energy should be considered, and several different multi-period stochastic programming also can be applied to enhance the resilient IPHS. For instance, [38] proposed a two-stage robust optimization model to coordinate the discrete and continuous reactive power compensators and find a robust optimal solution against any possible realization within the uncertain wind power output. Reference [39] proposed a two-stage robust centralized-optimal dispatch model to achieve a robust PV inverter dispatch solution considering the PV output uncertainties. And in [40], a novel day-ahead PV power forecasting approach based on deep learning was proposed and validated. Reference [41] established a total of 14 DYB models to estimate daily global solar radiation in six climate zones of China.

In this paper, a comprehensive multi-period restoration model (MPRM) is proposed for integrated power and hydrogen distribution system (IPHDS) under natural disasters with the coordination of RCs and MBCVs, and the dynamic delivery process of hydrogen is also taken into consideration.

The main contributions can be summarized as follows:
(i) We propose an IPHDS model, in which the power system and the hydrogen system are connected by electric hydrogen production devices (EHPs) and hydrogen-fired generators. Based on the aerodynamic laws, the dynamic hydrogen flow for the hydrogen delivery is applied in the IPHDS. To address the differential equations for the hydrogen dynamic flow, a differentiation and linearization method is also applied in this paper.
(ii) Based on the proposed IPHDS model, a multi-period restoration model is set up to improve the resilience of IPHDS, leveraging RCs and MBCVs to assist in system recovery of critical loads. Different from the existing research of RCs and MBCVs, the dynamic transportation state and ever-changing travel time for RCs and MBCVs are also taken into consideration in the proposed model.

The rest of the paper is summarized as follows. Section II details the modeling of three technologies: RCs, MBCVs, and dynamic hydrogen flow. Section III sets up the optimization of the MPRM model for the IPHDS with three technologies. Section IV studies and analyzes two cases for distribution network restoration. Finally, section V concludes this paper.

This article has been accepted for publication in a future issue of this journal, but has not been fully edited. Content may change prior to final publication. Citation information: DOI 10.1109/TIA.2021.3117926, IEEE Transactions on Industry Applications

II. Mathematical Modeling of RCs, MBCVs and Dynamic Hydrogen Flow

In this part, the models of RCs, MBCVs, and dynamic hydrogen flow are respectively set up for IPHDS restoration. Note that RCs and MBCVs have their own routes and are easily influenced by the transportation state. The transportation state and travel time variability are considered in the model of RCs and MBCVs.

Besides, since the hydrogen flow constraints are non-linear equalities and inequalities, a linearization method is used for the dynamic hydrogen flow to facilitate the computational burden.

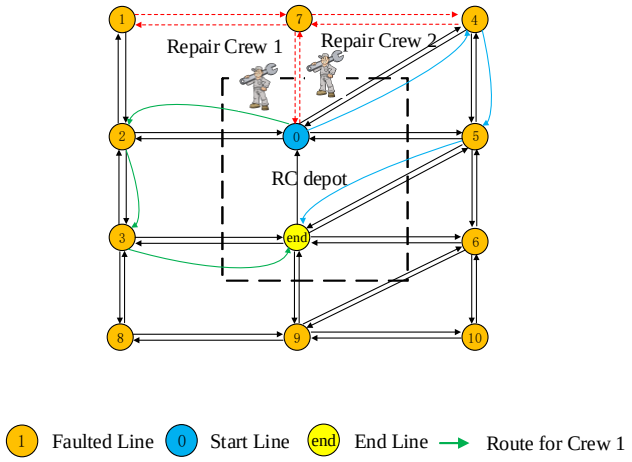

Fig. 1. An example of RC routes.

A. Modeling of Repair Crews

RCs are a kind of important resilient resources in IPHDS restoration. After the natural disaster happens, the RCs will be rapidly dispatched to faulted power branches and pipelines to perform the maintenance tasks. Reasonable routing and maintenance tasks of RCs can reduce the scheduling pressure of MBCVs. By collaboratively dispatching the RCs and MBCVs, the system outages can be effectively reduced, and the restoration speed will be clearly updated. In a restoration process, RCs can be modeled as a routing problem that can be formulated by the graph theory [46]. To explain the model of RCs, we assume that N lines are damaged in a natural disaster. Then, we can define a graph $H_K=(\Psi^{KA}, \Psi^{KL})$, and $\{0, 1, 2, 3, \dots, N, end\}$ is the index for the set of faulted lines, where "0" and "*end*" both represent the RC depot center. In a RC route, the repair crew should leave from the faulted line "0" to repair lines and return to faulted line "*end*" after repairing tasks. Fig. 1 shows an example of two RCs, including the travel routes of RC1 and RC2 which are $Route_1=\{0, 2, 3, end\}$ and $Route_2=\{0,4,5,end\}$. To guarantee that all RC routes start from "0" and return to "*end*" after repairing tasks are finished, we should have

$$\sum_{n\in\Psi^{KA}} M^{crew}_{0,n,c} - \sum_{m\in\Psi^{KA}} M^{crew}_{m,0,c} = 1, \forall c \tag{1}$$

$$\sum_{m\in\Psi^{KA}} M^{crew}_{m,end,c} - \sum_{n\in\Psi^{KA}} M^{crew}_{end,n,c} = 1, \forall c \tag{2}$$

where $M^{crew}_{0,n,c}$ is a binary variable that shows whether crew c travels from line 0 to line n. $M^{crew}_{m,0,c}$ is a binary variable that shows whether crew c travels from line m to line 0. $M^{crew}_{m,end,c}$ is a binary variable that shows whether crew c travels from line m to line *end*. $M^{crew}_{end,n,c}$ is a binary variable that shows whether crew c travels from line *end* to line n. For example, for RC1 in $Route_1$, we have $M^{crew}_{0,2,1}=M^{crew}_{2,3,1}=M^{crew}_{3,end,1}=1$, and others are 0. Ψ^{KA} denotes the set of the faulted lines. It worth noting that Ψ^{KA} contains not only faulted power branches, but also faulted hydrogen pipelines.

Moreover, the repair process should be continuous and each component should be repaired only once. Therefore, we have

$$R_{i,c} = \sum_{m\in\Psi^{KA}} M^{crew}_{m,i,c}, \forall i \in \Psi^{KA} \tag{3}$$

$$\sum_{\forall c} R_{i,c} = 1, \forall i \in \Psi^{KA} \tag{4}$$

where $R_{i,c}$ is a binary variable that indicates whether faulted line i is repaired by RC c. $M^{crew}_{m,i,c}$ is a binary variable that indicates whether RC c travels from m to i during the restoration.

Since each RC which leaves to repair a faulted line must return to the crew depot center after all repairing tasks, the number of RCs which leave each line should be equal to the number of RCs that arrive at this line. Thus, we have

$$\sum_{n\in\Psi^{KA}} M^{crew}_{s,n,c} - \sum_{m\in\Psi^{KA}} M^{crew}_{m,s,c} = 0, \forall s \in \Psi^{KA}, \forall c \tag{5}$$

where $M^{crew}_{s,n,c}$ is a binary variable that indicates whether RC c travels from s to n during the restoration. $M^{crew}_{m,s,c}$ is a binary variable that indicates whether RC c travels from m to s during the restoration.

Besides, the repair and travel time for each RC should also be formulated. To explain the time constraints for each RC, we still take Fig. 1 as an example. RC1 arrives at line 2 at $T^{crew}_{2,1} = T^{crew}_{0,1} + t_{0,2,l}$, $l = T^{crew}_{0,1}$, and arrives at faulted line 3 at $T^{crew}_{3,1} = T^{crew}_{2,1} + t^{crew}_{2,1} + t_{2,3,l}$, $l = T^{crew}_{2,1} + t^{crew}_{2,1}$. So, we can summarize that the faulted line m would be repaired and reconnected by the c-th RC after $T^{crew}_{m,c} + t^{crew}_{m,c}$. Thus, we have:

$$T^{crew}_{0,c} = 0, \forall c \tag{6}$$

$$-(1-M^{crew}_{m,n,c})M \le T^{crew}_{m,c} + t^{crew}_{m,c} + t_{m,n,l} - T^{crew}_{n,c} \le (1-M^{crew}_{m,n,c})M, \forall (m,n) \in \Psi^{KL}, \forall c, l = T^{crew}_{m,c} + t^{crew}_{m,c} \tag{7}$$

$$\sum_{\forall t} f^{m}_{i,t} = 1, \forall i \in \Psi^{KA} \tag{8}$$

$$\sum_{\forall t} \left(t \bullet f^{m}_{i,t}\right) \ge \sum_{\forall c} (T^{crew}_{i,c} + t^{crew}_{i,c} R_{i,c}), \forall i \in \Psi^{KA} \tag{9}$$

$$\sum_{\forall t} \left(t \bullet f^{m}_{i,t}\right) \le \sum_{\forall c} (T^{crew}_{i,c} + t^{crew}_{i,c} R_{i,c}) + 1 - \varepsilon, \forall i \in \Psi^{KA} \tag{10}$$

$$0 \le M^{crew}_{i,c} \le R_{i,c} M, \forall i \in \Psi^{KA}, \forall c \tag{11}$$

$$y_{s,r,t} \le \sum_{\tau=1}^{t-1} f^{m}_{i,\tau}, \forall i \in \Psi^{KA}, \forall c \tag{12}$$

where $T^{crew}_{0,c}$ denotes the time when crew c arrives at line 0. $T^{crew}_{m,c}$ denotes the time when crew c arrives at line m; $t^{crew}_{m,c}$ denotes the time for crew c to repair the line m. $t_{m,n,l}$ denotes the travel time for crew c from m to n at time l. Since the transportation state would be different at each time, the travel time for each road would be different according to the traffic congestion. $f^{m}_{i,t}$ is a binary variable that indicates at time t whether station i is repaired. ε denotes the error factor. t denotes the current time. $y_{s,r,t}$ is a binary variable indicating whether line (s, r) is connected at time t; 1 is "connected" and 0 otherwise. Ψ^{KL} denotes the set of the roads connected to faulted lines. Also, Ψ^{KL} contains the

roads connected to both faulted power branches and pipelines. Constraints (6)-(12) are crew time limits. Constraint (6) ensures that all crews start from the depot (marked as 0) immediately after the outage (t = 0). Constraint (7) is a big-M constraint to define the arrival time for each point in the graph. In constraint (7), we assume that a RC arriving at a faulted line will complete the line repair before departure. When $M^{crew}_{m,n,c}$=1, RC c travels from m to n, spends $t_{m,n,l}$, $l = T^{crew}_{m,c} + t^{crew}_{m,c}$ on travel, and completes the repair at $t^{crew}_{i,c}$. And when $M^{crew}_{m,n,c} \neq 1$, M is defined as a large number so that the variables are affected. Constraint (8) implies that each faulted line would be repaired only once; $f^{m}_{i,t}$ means that the faulted line i repair is completed and the line is ready to be energized at time t. Constraints (9) and (10) combine the binary variable $f^{m}_{i,t}$ with integer variable $T^{crew}_{i,c}$ to limit the repair time for each faulted line. Constraint (11) guarantees that only crew c, which was used to repair line i, has a positive value of $T^{crew}_{i,c}$; otherwise, the sum of $T^{crew}_{i,c}$ for each crew c will not represent the time the crew arrives at faulted line i. Constraint (12) ensures that the line can be energized in the distribution system after the repair, and (8) ensures that every faulted lines would be repaired.

B. Modeling of Mobile Battery-Carried Vehicles

When an outage happens, MBCVs will be dispatched from the vehicle depot center to the charging station to support critical loads, especially the loads located in an island. After the critical loads are restored, the MBCV should travel to another charging station to support other loads. Similar to the RCs, the model of MBCVs can also be formulated by graph theory. Also, we can define a graph H_G=(Ψ^{GA}, Ψ^{GL}) with N charging stations, and {0, 1, 2, 3, … , N, *end*} is the index for the set of charging station nodes, where "0" and "*end*" both represent the vehicle depot center. In an MBCV route, the MBCV should leave from the vehicle charging station "0" to support critical loads and return to the charging station "*end*" after the charging tasks. Also, to guarantee that all MBCVs start from "0" and return to "*end*" after the charging tasks are finished, there should be

$$\sum_{n\in\Psi^{GA}} M^{vehicle}_{o,n,d} - \sum_{m\in\Psi^{GA}} M^{vehicle}_{m,0,d} = 1, \forall d \tag{13}$$

$$\sum_{m\in\Psi^{GA}} M^{vehicle}_{m,end,d} - \sum_{n\in\Psi^{GA}} M^{vehicle}_{end,n,d} = 1, \forall d \tag{14}$$

where $M^{vehicle}_{0,n,d}$ is a binary variable that shows whether MBCV d travels from station 0 to station n. $M^{vehicle}_{m,0,d}$ is a binary variable that shows whether MBCV d travels from station m to station 0. $M^{vehicle}_{m,end,d}$ is a binary variable that shows whether MBCV d travels from station m to station *end*. $M^{vehicle}_{end,n,d}$ is a binary variable that shows whether MBCV d travels from station *end* to station n. Ψ^{GA} denotes the set of stations with plugs to MBCV.

Similarly, MBCVs that come to a charging station must leave when charging is completed, which leads to

$$\sum_{n\in\Psi^{GA}} M^{vehicle}_{s,n,d} - \sum_{m\in\Psi^{GA}} M^{vehicle}_{m,s,d} = 0, \forall s \in \Psi^{GA}, \forall d \tag{15}$$

Though there are many similar parts in the RC and MBCV models, there still exist three differences. Note that MBCVs can only support power load at the charging station and cannot repair the faulted stations and lines. Therefore, functions (3) and (4) are not applied in the MBCV model. On the other hand, in the RC model, only one RC can repair a faulted line simultaneously. But in the model for MBCVs, it is normal that several MBCVs arrive at the same charging station, which means function (8) is not necessary in the MBCV model. Besides, the charging time of MBCVs at each station can be varied according to the demand, while the repair time for RCs at each faulted line is fixed. Thus, the charging and travel time constraints for MBCVs should be expressed as

$$T^{vehicle}_{n,d} = T^{vehicle}_{m,d} + t^{MBCV}_{m,n,d,l} + t^{vehicle}_{m,d}, \quad \forall d, l = T^{vehicle}_{m,d} + t^{vehicle}_{m,d} \tag{16}$$

where $T^{vehicle}_{n,d}$ denotes the time when vehicle d arrives at the station n. $T^{vehicle}_{m,d}$ denotes the time when vehicle d arrives at station m. $t^{MBCV}_{m,n,d,l}$ denotes the travel time of MBCV d from m to n at time l. $t^{vehicle}_{m,d}$ denotes the time when vehicle d stays at station m. To characterize the relationship between $T^{vehicle}_{m,c}$ and $t^{MBCV}_{m,n}$, a big-M approach is employed by [47],where

$$\begin{aligned} -(1-M^{vehicle}_{m,n,d})M \le T^{vehicle}_{m,d} + t^{vehicle}_{m,d} + t^{MBCV}_{m,n,d,l} - T^{vehicle}_{n,d} \\ \le (1-M^{vehicle}_{m,n,d})M, \forall (m,n) \in \Psi^{GL}, \\ \forall d, l = T^{vehicle}_{m,d} + t^{vehicle}_{m,d} \end{aligned} \tag{17}$$

Moreover, MBCVs satisfy the following operation constraints

$$T^{vehicle}_{0,d} = 0, \forall d \tag{18}$$

$$\sum_{\forall t} f^{c}_{i,t,d} \le 1, \forall i \in \Psi^{GA}, \forall d \tag{19}$$

$$\sum_{\forall t} f^{c}_{i,t,d} = \sum_{\forall t} l^{c}_{i,t,d}, \forall i \in \Psi^{GA}, \forall d \tag{20}$$

$$T^{vehicle}_{i,d} \le \sum_{\forall t} \left(t \bullet f^{c}_{i,t,d}\right) \le T^{vehicle}_{i,d} + 1 - \varepsilon, \forall i \in \Psi^{GA}, \forall d \tag{22}$$

$$\sum_{\forall t} \left(t \bullet l^{c}_{i,t,d}\right) \le T^{vehicle}_{i,d} + t^{vehicle}_{i,d} + 1 - \varepsilon, \forall i \in \Psi^{GA}, \forall d \tag{23}$$

$$t^{vehicle}_{i,d} \ge 0, \forall i \in \Psi^{GA}, \forall d \tag{24}$$

$$0 \le T^{vehicle}_{i,d} \le M \sum_{m\in\Omega^{GA}} M^{vehicle}_{m,i,d}, \forall i \in \Psi^{GA}, \forall d \tag{25}$$

where $f^{c}_{i,t,d}$ is a binary variable that indicates whether vehicle d arrives at station i at time t. $l^{c}_{i,t,d}$ is a binary variable that indicates whether vehicle d leaves the station at time t i. Constraint (18) ensures that all vehicles start from the depot at time 0. Constraint (19) indicates that a station is visited only once by each MBCV. Constraint (20) suggests that one MBCV should leave the station only if it visits the station. Constraints (21)-(23) are similar to (9) and (10), coupling the binary variables ($f^{c}_{i,t,d}$, $l^{c}_{i,t,d}$) with the integer variables ($T^{vehicle}_{i,d}$, $t^{vehicle}_{i,d}$). Constraint (24) indicates that the MBCV stay time is non-negative. In addition, constraint (25) makes sure that vehicle arrive time is equal to 0 if vehicle d did not visit the station.

C. Model of IPHDS and Hydrogen Dynamic Flow

Fig. 2 shows an illustration of an IPHDS, where the hydrogen system and power distribution system are connected with each other by hydrogen-fired generators and EHPs. The hydrogen-fired generators generate electricity by burning hydrogen. And the hydrogen-fired generators are the power source in the power distribution system, while they are also hydrogen loads in the hydrogen system. On the contrary, the EHPs are the hydrogen sources in the hydrogen system, while they are electric load in the power distribution system.

When the power system is integrated with a hydrogen system, the hydrogen-fired generators will be wildly utilized as an important coupling component in the IPHDS. The hydrogen-fired

generators generate electricity by burning hydrogen gas. Technically, the operation parameters of the coal-fired generators and hydrogen-fired generators are quite different, and the difference between the modeling of coal-fired generators and hydrogen-fired generators mainly lies in two aspects. On the one hand, the ramping rates and minimum technical generations of the coal-fired and hydrogen-fired generators are different. On the other hand, the coal-fired generators are only the generation components in the power system, while the hydrogen-fired generators not only generate electricity in the power system but also consume hydrogen gas in the hydrogen system.

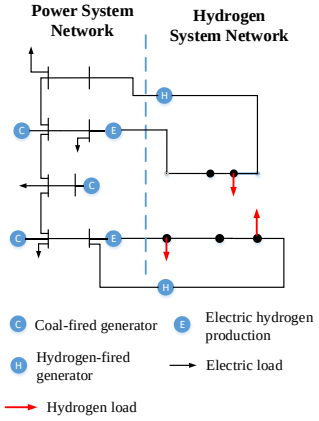

Fig. 2 An illustration of the IPHDS

The distribution power system is applied in this paper, and the power flow equations in the distribution power system can be expressed as

$$\begin{cases} P_{c,t}+P_{h,t}-P^{e}_{j,t}-P_{q,\mathrm{EHP},t}= \\ \sum_{\forall s\in\delta_t(j)} H_{js,t}-\sum_{\forall i\in\pi_t(j)} H_{ij,t} \\ Q_{c,t}+Q_{h,t}-Q_{j,t}-Q_{q,\mathrm{EHP},t}= \\ \sum_{\forall s\in\delta_t(j)} G_{js,t}-\sum_{\forall i\in\pi_t(j)} G_{ij,t} \\ \forall c\in\mathcal{D},\forall h\in\mathcal{L},\forall j\in\mathcal{E},\forall q\in\Omega,\forall t=1,...,T \end{cases}, \quad (27)$$

$$\begin{cases} -M\cdot\left(1-y_{i,j,t}\right)\le V_{j,t}-V_{i,t}-\left(r_{ij}H_{ij,t}+x_{ij}G_{ij,t}\right) \\ \qquad\le M\cdot\left(1-y_{i,j,t}\right) \\ H^{2}_{ij,t}+G^{2}_{ij,t}\le S^{\max}_{ij}y_{i,j,t} \\ \forall(i,j)\in\mathcal{Y}\cup\mathbb{U},\forall t=1,...,T \end{cases}, \quad (28)$$

$$Q_{j,t}=\tan\theta_{j,t}P^{e}_{j,t},\forall j\in\mathcal{E},\forall t=1,...,T \quad (29)$$

where $P_{c,t}$ and $Q_{c,t}$ are the active and reactive powers of the coal-fired generator connected to bus c at time period t; $P_{h,t}$ and $Q_{h,t}$ are the active and reactive powers of the hydrogen-fired generator connected to bus h at time period t; $P_{q,\mathrm{EHP},t}$ is the active power consumption of the EHP connected to bus q at time period t; $H_{js,t}$ and $G_{js,t}$ are the active and reactive powers on the power branch (j, s) at time period t; $V_{j,t}$ is the voltage magnitude of bus j at time period t; $\theta_{j,t}$ is the voltage phase angle of bus j at time period t; $P^{e}_{j,t}$ and $Q_{j,t}$ are the active and reactive loads of bus j at time period t; $\delta_t(j)$ and $\pi_t(j)$ are the sets of child buses and parent buses of bus j at time period t; $\mathcal{E}$ denotes the set of electric buses; $\mathcal{D}$ denotes the set of electric buses connected with coal-fired generators; $\mathcal{L}$ denotes the set of electric buses connected with the hydrogen-fired generators. $\mathbb{U}$ is the set of the backup reconfigured power branches. Ω is the set of the buses connected with EHPs. (28) denotes the power balance constraint at each bus in the power system. (29) indicates that the power factor of each bus should be kept within a specified value at each time period. (30) specifies the voltage drop on each power branch.

In this paper, the distribution hydrogen system consists of three major components, including EHPs, hydrogen-fired generators, and hydrogen transmission pipelines. The models of key hydrogen components are described as follows.

Different from the electricity delivery in power branches, the hydrogen delivery in hydrogen pipelines follows the aerodynamic laws, and the hydrogen flow will be driven by the pressure along the pipelines in correspondence to the ingredients, temperature, density, etc.

To visually illustrate the modeling of a hydrogen pipeline, Fig. 3 presents a graphical illustration about a typical hydrogen pipeline with the corresponding internal parameters.

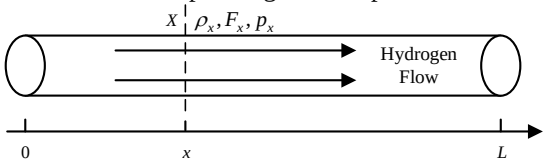

Fig. 3 An illustration of a hydrogen pipeline

In Fig. 3, if we take the leftmost end of the pipeline as the starting point, a coordinate axis can be easily created with the leftmost end of the pipeline as the origin. As a result, the rightmost coordinate of the pipeline is L. For each point in the pipeline, the coordinate of this point can be determined by the distance of this point from the starting point. Therefore, for the point X in Fig. A-1, the coordinate of this point is x, which also denotes the distance of point X from the starting point. The hydrogen density, hydrogen mass flow rate, and hydrogen pressure also can be shown as ρ_x, F_x, and p_x.

The hydrogen states such as velocity, temperature, density, pressure, etc. can be linked by the one-dimensional fluid dynamics along the pipelines. Generally, according to the aerodynamic criteria, the process can be described by the following two equations [47]:

$$\frac{\partial\rho}{\partial t}+\frac{\partial F}{A\partial x}=0 \quad (30)$$

$$\frac{\partial F}{A\partial t}+\frac{\partial p}{\partial x}+\frac{\lambda}{2d}\frac{F^{2}}{\rho A^{2}}=0 \quad (31)$$

where ρ refers to the hydrogen density; F denotes the hydrogen mass flow rate; p denotes the hydrogen pressure; t denotes to the operation time; x denotes the coordinate of each point in a pipeline; A denotes the cross-sectional area of the pipelines; d denotes the diameter of the pipeline; λ denotes the friction coefficient of the pipeline.

Since (30) and (31) are partial differential equations and difficult to be solved, they need to be turned into their difference form. Here, the partial differential equations (30) and (31) are

This article has been accepted for publication in a future issue of this journal, but has not been fully edited. Content may change prior to final publication. Citation information: DOI 10.1109/TIA.2021.3117926, IEEE Transactions on Industry Applications

approximately transformed in the following *Wendroff* difference form [44, 45], where each partial differential equation is reformulated by $X_{i+1,t+1}$, $X_{i,t+1}$, $X_{i+1,t}$ and, $X_{i,t}$.

$$\begin{aligned}\frac{\partial X}{\partial t}&=\frac{1}{2}\left(\frac{X_{i+1,t+1}-X_{i+1,t}}{\Delta t}+\frac{X_{i,t+1}-X_{i,t}}{\Delta t}\right)+O(x^2+t^2)\\&\approx\frac{1}{2}\left(\frac{X_{i+1,t+1}-X_{i+1,t}}{\Delta t}+\frac{X_{i,t+1}-X_{i,t}}{\Delta t}\right)\end{aligned}\tag{32}$$

$$\begin{aligned}\frac{\partial X}{\partial x}&=\frac{1}{2}\left(\frac{X_{i+1,t+1}-X_{i+1,t}}{\Delta x}+\frac{X_{i,t+1}-X_{i,t}}{\Delta x}\right)+O(x^2+t^2)\\&\approx\frac{1}{2}\left(\frac{X_{i+1,t+1}-X_{i+1,t}}{\Delta x}+\frac{X_{i,t+1}-X_{i,t}}{\Delta x}\right)\end{aligned}\tag{33}$$

$$\begin{aligned}X&=\frac{1}{4}\left(X_{i+1,t+1}+X_{i,t+1}+X_{i+1,t}+X_{i,t}\right)+O(x^2+t^2)\\&\approx\frac{1}{4}\left(X_{i+1,t+1}+X_{i,t+1}+X_{i+1,t}+X_{i,t}\right)\end{aligned}\tag{34}$$

where Δt and Δx indicate the time and spatial step, respectively. The second order accuracy with the truncation errors $O(\Delta t^2+\Delta x^2)$ in (32)-(34) are ignored in this paper.

According to the *Wendroff* difference form, the partial differential equations (30) and (31) can be transformed into (35) and (36), and the transient mass flow in the hydrogen pipelines can be simply expressed by (35)-(36).

$$\left(\rho_{i+1,t+1}+\rho_{i,t+1}-\rho_{i+1,t}-\rho_{i,t}\right)+\frac{\Delta t}{\Delta xA}\left[F_{i+1,t+1}+F_{i+1,t}-F_{i,t+1}-F_{i,t}\right]=0\tag{35}$$

$$\begin{aligned}&\frac{1}{A}\left[F_{i+1,t+1}+F_{i,t+1}-F_{i+1,t}-F_{i,t}\right]+\\&+\frac{\Delta t}{\Delta x}\left[p_{i+1,t+1}+p_{i+1,t}-p_{i,t+1t}-p_{i,t}\right]\\&+\frac{\lambda\Delta x}{4dA}\left(\frac{F_{i,t+1}^2}{\rho_{i,t+1}}+\frac{F_{i+1,t+1}^2}{\rho_{i+1,t+1t}}+\frac{F_{i+1,t}^2}{\rho_{i+1,t}}+\frac{F_{i,t}^2}{\rho_{i,t}}\right)=0\end{aligned}\tag{36}$$

Thus, inspecting the hydrogen flow in pipeline (m, n) gives

$$\begin{aligned}&\left(\rho_{mn,i+1,t+1}+\rho_{mn,i,t+1t}-\rho_{mn,i+1,t}-\rho_{mn,i,t}\right)+\\&\frac{\Delta t}{\Delta xA_{mn}}\begin{bmatrix}F_{mn,i+1,t+1}+F_{mn,i+1,t}\\-F_{mn,i,t+1}-F_{mn,i,t}\end{bmatrix}=0,\\&\forall t=1,\ldots,T-1,\forall i=0,\ldots,\left[\frac{L_{mn}}{\Delta x}\right]-1\end{aligned}\tag{37}$$

$$\begin{aligned}&\frac{1}{A_{mn}}\left[F_{mn,i+1,t+1}+F_{mn,i,t+1}-F_{mn,i+1,t}-F_{mn,i,t}\right]+\\&+\frac{\Delta t}{\Delta x}\left[p_{mn,i+1,t+1}+p_{mn,i+1,t}-p_{mn,i,t+1}-p_{mn,i,t}\right]\\&+\frac{\lambda\Delta x}{4dA_{mn}}\begin{pmatrix}\frac{F_{mn,i,t+1}^2}{\rho_{mn,i,t+1}}+\frac{F_{mn,i+1,t+1}^2}{\rho_{mn,i+1,t+1}}\\+\frac{F_{mn,i+1,t}^2}{\rho_{mn,i+1,t}}+\frac{F_{mn,i,t}^2}{\rho_{mn,i,t}}\end{pmatrix}=0,\\&\forall t=1,\ldots,T-1,\forall i=0,\ldots,\left[\frac{L_{mn}}{\Delta x}\right]-1\end{aligned}\tag{38}$$

where L_{mn} denotes the length of pipeline (m, n).

Note that constraint (38) is a non-linear function and cannot be solved by convex optimization method. Thus, the relationship among hydrogen density ρ, hydrogen mass flow rate F, and hydrogen velocity w is applied as [46].

$$F=A\cdot\rho\cdot w\tag{39}$$

Since the hydrogen velocity wouldn't change too much in the operation state, the second-order term in (38) can be approximately changed into

$$\begin{aligned}&\frac{\lambda\Delta x}{4dA_{mn}}\begin{pmatrix}\frac{F_{mn,i,t+1}^2}{\rho_{mn,i,t+1}}+\frac{F_{mn,i+1,t+1}^2}{\rho_{mn,i+1,t+1}}\\+\frac{F_{mn,i+1,t}^2}{\rho_{mn,i+1,t}}+\frac{F_{mn,i,t}^2}{\rho_{mn,i,t}}\end{pmatrix}\\&=\frac{\lambda\Delta x}{4dA_{mn}}\begin{pmatrix}\frac{A_{mn}\rho_{mn,i,t+1}w_{mn,i,t+1}F_{mn,i,t+1}}{\rho_{mn,i,t+1}}\\+\frac{A_{mn}\rho_{mn,i+1,t+1}w_{mn,i+1,t+1}F_{mn,i+1,t+1}}{\rho_{mn,i+1,t+1}}\\+\frac{A_{mn}\rho_{mn,i+1,t}w_{mn,i+1,t}F_{mn,i+1,t}}{\rho_{mn,i+1,t}}\\+\frac{A_{mn}\rho_{mn,i,t}w_{mn,i,t}F_{mn,i,t}}{\rho_{mn,i,t}}\end{pmatrix}\\&\approx\frac{\lambda\Delta x}{4dA_{mn}}\begin{pmatrix}\frac{A_{mn}\rho_{mn,i,t+1}\overline{w_{mn}}F_{mn,i,t+1}}{\rho_{mn,i,t+1}}\\+\frac{A_{mn}\rho_{mn,i+1,t+1}\overline{w_{mn}}F_{mn,i+1,t+1}}{\rho_{mn,i+1,t+1}}\\+\frac{A_{mn}\rho_{mn,i+1,t}\overline{w_{mn}}F_{mn,i+1,t}}{\rho_{mn,i+1,t}}\\+\frac{A_{mn}\rho_{mn,i,t}\overline{w_{mn}}F_{mn,i,t}}{\rho_{mn,i,t}}\end{pmatrix}\\&=\frac{\lambda\Delta x\overline{w_{mn}}}{4d}\begin{pmatrix}F_{mn,i,t+1}+F_{mn,i+1,t+1}\\+F_{mn,i+1,t}+F_{mn,i,t}\end{pmatrix},\\&\forall t=1,\ldots,T-1,\forall i=0,\ldots,\left[\frac{L_{mn}}{\Delta x}\right]-1\end{aligned}\tag{40}$$

where $\overline{w_{mn}}$ denotes the average hydrogen velocity in pipeline (m, n). Thus, equation (38) can be linearized into (41).

This article has been accepted for publication in a future issue of this journal, but has not been fully edited. Content may change prior to final publication. Citation information: DOI 10.1109/TIA.2021.3117926, IEEE Transactions on Industry Applications

$$\begin{aligned}&\frac{1}{A_{mn}}\left[F_{mn,i+1,t+1}+F_{mn,i,t+1}-F_{mn,i+1,t}-F_{mn,i,t}\right]\\&+\frac{\Delta t}{\Delta x}\left[p_{mn,i+1,t+1}+p_{mn,i+1,t}-p_{mn,i,t+1}-p_{mn,i,t}\right]\\&+\frac{\lambda\Delta x\overline{w_{mn}}}{4d}\begin{pmatrix}F_{mn,i,t+1}+F_{mn,i+1,t+1}\\+F_{mn,i+1,t}+F^2_{mn,i,t}\end{pmatrix}=0\\&\forall t=1,...,T-1,\forall i=0,...,\left[\frac{L_{mn}}{\Delta x}\right]-1\end{aligned},\tag{41}$$

To ensure the balance of hydrogen flow at each hydrogen node, the hydrogen flow should follow the equation below.

$$\begin{aligned}&K_{i,t}-F^{g}_{n,t}-K_{b,t}\\&=\sum_{\forall o\in\alpha_t(n)}F_{no,0,t}-\sum_{\forall m\in\beta_t(n)}F_{mn,\mathrm{end},t},\\&\forall n\in\mathcal{Q},\forall i\in\gamma,\forall b\in\Pi,\forall t=1,...,T\end{aligned}\tag{42}$$

where $K_{i,t}$ denotes the hydrogen output of EHP connected to node i at time period t; $K_{b,t}$ denotes the consumption of hydrogen-fired generator connected to node b at time period t; $F^{g}_{n,t}$ denotes the hydrogen load connected to node n at time period t. $\alpha_t(n)$ and $\beta_t(n)$ are the sets of child and parent nodes of node n at time period t; $\mathcal{Q}$ is the set of hydrogen nodes; γ is the set of hydrogen nodes connected to the EHPs. Π is the set of hydrogen nodes connected to the hydrogen-fired generators.

The EHPs and hydrogen-fired generators are the major coupling components in the IPHDS. The electricity and hydrogen conversion equations of the EHPs and hydrogen-fired generators can be expressed as follows.

$$\begin{aligned}&K_{i,t}=\eta_{i,q}\cdot P_{q,\mathrm{EHP},t},\\&\forall q\in\Omega,\forall i\in\gamma,\forall t=1,...,T\end{aligned}\tag{43}$$

$$\begin{aligned}&K_{b,t}=P_{h,t}/GHV,\\&\forall h\in\mathcal{L},\forall b\in\Pi,\forall t=1,...,T\end{aligned}\tag{44}$$

where $\eta_{i,q}$ is the conversion factor of EHP allocated at hydrogen node i and electric bus q, and GHV is the hydrogen gross heating value.

III. Formulation of the Restoration Process

In this section, a multi-period restoration model for IPHDS considering dynamic hydrogen flow is proposed to maximize the total restored weighted loads. The model aims to determine the optimal routes for RCs and MBCVs as well as the network reconfiguration with the consideration of the transportation states. The optimization model can be set up as follows.

A. Objective Function

The objective of the MPRM is to quickly pick up critical loads. By properly choosing the weights, we can ensure that high-priority loads are restored first. Mathematically, the objective function is expressed as the sum of weighted loads:

$$obj=\max\left(\sum_{\forall t}\sum_{\forall j}z^{e}_{j}\frac{P^{e}_{j,t}}{P^{e}_{\max,j}}+\sum_{\forall t}\sum_{\forall n}z^{g}_{n}\frac{F^{g}_{n,t}}{F^{g}_{\max,n}}\right)\tag{45}$$

where $P^{e}_{j,t}$ and $F^{g}_{n,t}$ denote the restored active power at bus j and restored hydrogen load at node n at time t, respectively; z^{e}_{j} and z^{g}_{n} denote the power load weight and hydrogen load weight, respectively; $P^{e}_{max,j}$ and $F^{g}_{max,n}$ denote the upper bound of power load and hydrogen load, respectively.

B. Constraints

The constraints of the model should satisfy the requirement of the secure system operation. Specifically, these constraints will include

1) Power flow constraints

The MPRM for the IPHDS should maintain power flow balance at each time period without the violation of physical limits,

$$(27)\text{-}(29)\tag{46}$$

$$\begin{aligned}&V^{\min}_{j}\le V_{j,t}\le V^{\max}_{j},\\&\forall j\in\mathcal{E},\forall t=1,...,T\end{aligned}\tag{47}$$

$$\begin{aligned}&V_{j,t}=V^{0}_{j},\\&\forall j\in\mathcal{D}\cup\mathcal{L},\forall t=1,...,T\end{aligned}\tag{48}$$

$$\begin{cases}P^{\min}_{c}\le P_{c,t}\le P^{\max}_{c}\\Q^{\min}_{c}\le Q_{c,t}\le Q^{\max}_{c}\\P^{\min}_{h}\le P_{h,t}\le P^{\max}_{h}\\Q^{\min}_{h}\le Q_{h,t}\le Q^{\max}_{h}\end{cases},\forall c\in\mathcal{D},\forall h\in\mathcal{L},\forall t=1,...,T\tag{49}$$

$$\begin{aligned}&\begin{cases}r^{\min}_{c}\le P_{c,t+1}-P_{c,t}\le r^{\max}_{c}\\r^{\min}_{h}\le P_{h,t+1}-P_{h,t}\le r^{\max}_{h}\end{cases},\\&\forall c\in\mathcal{D},\forall h\in\mathcal{L},\forall t=1,...,T-1\end{aligned}\tag{50}$$

$$\begin{cases}P^{\min}_{q,\mathrm{EHP}}\le P_{q,\mathrm{EHP},t}\le P^{\max}_{q,\mathrm{EHP}}\\Q^{\min}_{q,\mathrm{EHP}}\le Q_{q,\mathrm{EHP},t}\le Q^{\max}_{q,\mathrm{EHP}}\end{cases},\forall q\in\Omega,\forall t=1,...,T\tag{51}$$

$$(1)\text{-}(25)\tag{52}$$

where $P^{\min}_{q,\mathrm{EHP}}$ and $P^{\max}_{q,\mathrm{EHP}}$ are the lower and upper bounds of the active power of the EHP connected to bus q; $Q^{\min}_{q,\mathrm{EHP}}$ and $Q^{\max}_{q,\mathrm{EHP}}$ are the lower and upper bounds of the reactive power of the EHP connected to bus q; $P^{\min}_{c}$ and $P^{\max}_{c,}$ are the lower and upper bounds of the active power of the coal-fired generator connected to bus c ; $Q^{\min}_{c}$ and $Q^{\max}_{c,}$ are the lower and upper bounds of the reactive power of the coal-fired generator connected to bus c ; $P^{\min}_{h}$ and $P^{\max}_{h,}$ are the lower and upper bounds of the active power of the hydrogen-fired generator connected to bus h ; $Q^{\min}_{h}$ and $Q^{\max}_{h,}$ are the lower and upper bounds of the reactive power of the hydrogen-fired generator connected to bus c ; $r^{\min}_{c}$ and $r^{\max}_{c}$ are the lower and upper bounds of the coal-fired generators ramping rate; $r^{\min}_{h}$ and $r^{\max}_{h}$ are the lower and upper bounds of the hydrogen-fired generators ramping rate; $V^{\min}_{j}$ and $V^{\max}_{j}$ are the lower and upper bounds of the voltage magnitude at bus j; V^{0}_{j} is the specified voltage magnitude at bus j.

For these constraints in the power system, we assume that the power system and hydrogen system are coupled by hydrogen-fired generators and EHPs. Moreover, constraint (46) denotes the limitations for the power flow balance. Constraint (47) specifies the upper and lower bounds of the voltage magnitude at each bus, and constraint (48) indicates that the voltage magnitude for the bus connected with coal-fired generators or hydrogen-fired generators will always be specified as the given value. Constraint (49) denotes the power consumption limit of EHPs. Constraints (50) and (51) specify the upper and lower bounds of coal-fired generators and hydrogen-fired generators. (52) is the constraint for RCs and MBCVs.

2) Hydrogen flow constraints

In the hydrogen system, the MPRM should maintain hydrogen balance and physical limits, giving

$$F_{mn}^{\min} \cdot y_{m,n,t} \le F_{mn,i,t} \le F_{mn}^{\max} \cdot y_{m,n,t}, \quad \forall (m,n) \in \mathcal{P} \cup \mathbb{B}, \forall t = 1,...,T, \quad \forall i = 0,...,\left\lfloor \frac{L_{mn}}{\Delta x} \right\rfloor \tag{53}$$

$$p_{mn}^{\min} \le p_{mn,i,t} \le p_{mn}^{\max}, \forall (m,n) \in \mathcal{P} \cup \mathbb{B}, \quad \forall t = 1,...,T, \forall i = 0,1,...,\left\lfloor \frac{L_{mn}}{\Delta x} \right\rfloor \tag{54}$$

$$\rho_{mn}^{\min} \le \rho_{mn,i,t} \le \rho_{mn}^{\max}, \forall (m,n) \in \mathcal{P} \cup \mathbb{B}, \quad \forall t = 1,...,T, \forall i = 0,...,\left\lfloor \frac{L_{mn}}{\Delta x} \right\rfloor \tag{55}$$

(42)-(44) (56)

(37), (41) (57)

where F_{mn}^{min} and F_{mn}^{max} are the lower and upper bounds of the hydrogen mass flow rate in pipeline (m, n); p_{mn}^{min} and p_{mn}^{max} are the lower and upper bounds of the hydrogen pressure in pipeline (m, n); ρ_n^{min} and ρ_n^{max} denote the lower and upper bounds of the hydrogen density in pipeline (m, n).

For these constraints in the hydrogen system, we assume that the hydrogen loads are only supplied by EHPs, and the hydrogen flow will be dynamically changed in pipelines. Moreover, constraint (53) denotes the limit of the hydrogen mass flow rate. Constraint (54) denotes the limit of the hydrogen pressure for each pipeline. Constraint (55) denotes the limit of hydrogen density for each pipeline. Constraint (56) denotes the hydrogen flow balance, and conversion relationship between EHPs and hydrogen-fired generators. Constraint (57) gives the dynamic hydrogen flow for each pipeline.

3) Network reconfiguration constraints

To improve the resilience of IPHDS, the network reconfiguration strategy has been adopted in the MPRM, yielding the following constraints:

$$y_{i,j,t} = u_{i,j,t}, \forall (i,j) \in \mathbb{U}, \forall t = 1,...,T \tag{58}$$

$$\sum_{\forall (i,j) \in \mathbb{U}} u_{i,j,t} \le u_t^{\max}, \forall t = 1,...,T \tag{59}$$

$$\sum_{\forall t} u_{i,j,t} \le 1, \forall (i,j) \in \mathbb{U} \tag{60}$$

$$y_{m,n,t} = r_{m,n,t}, \forall (m,n) \in \mathbb{B}, \forall t = 1,...,T \tag{61}$$

$$\sum_{\forall (m,n) \in \mathbb{B}} r_{m,n,t} \le r_t^{\max}, \forall t = 1,...,T \tag{62}$$

$$\sum_{\forall t} r_{m,n,t} \le 1, \forall (m,n) \in \mathbb{B} \tag{63}$$

where $u_{i,j,t}$ is a binary variable indicating whether power line (i, j) is reconfigured at time period t: if it is reconfigured, $u_{i,j,t}$ =1; 0 otherwise. $r_{m,n,t}$ is a binary variable which indicates whether pipeline (m, n) is reconfigured at time period t; u_t^{max} denotes the maximum number of the reconfigured power branches at time period t; $r_{l,t}^{max}$ denotes the maximum number of the reconfigured pipelines at time period t. Functions (58) and (61) are the reconfiguration state constraints, denoting that if a power line or pipeline is reconfigured, it would follow the power flow constraints and the hydrogen flow constraints. Constraints (59) and (62) shows the limits of reconfigured power branches and pipelines at each time period. Constraints (60) and (63) indicate that each power line or pipeline should only be reconfigured once during an outage.

Therefore, the MPRM for IPHDS can be finally set up with the objective function (45), subject to power system constraints (46)-(52), hydrogen system constraints (53)-(57), and network reconfiguration constraints (58)-(63).

IV. Case Studies

In this section, two different IPHDSs are employed to shown the effectiveness of the proposed model. The first IPHDS is integrated by a modified IEEE 33-bus distribution system and a 48-node hydrogen system. The other IPHDS is integrated by a 144-bus distribution system and three hydrogen systems containing 85 different hydrogen nodes.

1) IPHDS integrated by a modified IEEE 33-bus distribution system and a 48-node hydrogen system

The IPHDS integrated by a modified IEEE 33-bus distribution system and a 48-node hydrogen system is employed to show the effectiveness of the proposed model, the topology of which is depicted in Fig. 4. In Fig. 4, the faulted lines are denoted by "×". Power buses 1, 15 and 29 are connected with coal-fired generators, and power buses 6, 9, 17, 21 and 23 are connected with hydrogen nodes 9, 7, 20, 24 and 37 by hydrogen-fired generators, respectively. Besides, we prioritize all power loads into five levels, demonstrating the load priority in [48]. The power loads with the highest priority are located at buses 4, 19, 25, while the power loads with the second-highest priority are located at buses 9, 26, 27.

In the 48-node hydrogen system, source nodes 2, 11, 16, 23 and 39 are connected to power buses 3, 16, 19, 25 and 30 by EHPs, respectively. Other nodes are all connected with hydrogen loads. Similarly, hydrogen loads are also prioritized into five levels, with hydrogen loads at nodes 4 and 15 being prioritized the highest level, and loads at nodes 1 and 18 being prioritized the second-highest level. Note that nodes 7, 9, 20, 24 and 37 are connected with the power distribution system via hydrogen-fired generators. To guarantee the hydrogen supply, the loads at nodes 7 and 20 also have the highest priority.

To quantify the restoration performance, the load restoration time is defined as the total required time to recover the load. Besides, we assume that there are two RCs and two MBCVs in the power system, and two RCs in the hydrogen system. The time for each RC to repair the faults is shown in Table I and Table II. Moreover, the travel time for each RC and MBCV among faulted lines is detailed in [48].

The optimal RC and MBCV routes are also depicted in Fig. 4. Once the faulted lines are repaired, the islands will be re-connected and the loads will be restored. In the power distribution system, the fault power branches closer to the RC depot, such as Fault 1 and Fault 3, will be first repaired by RC1 and RC2, respectively. Next, Fault 5 will be repaired by RC1, while Fault 3, Fault 2 and Fault 4 will be repaired by RC2 in sequence.

TABLE I Repair Time of RCs in the 33-Bus System

Outages	Repair time (minutes)	
	Repair Crew 1	Repair Crew 2
Fault 1	120	60
Fault 2	120	60

Fault 3	60	120
Fault 4	60	60
Fault 5	120	60

TABLE II REPAIR TIME OF RCS IN THE 48-NODE SYSTEM

Outages	Repair time (minutes)	
	Repair Crew 3	Repair Crew 4
Fault 6	60	60
Fault 7	180	120
Fault 8	120	120
Fault 9	120	60
Fault 10	60	60
Fault 11	120	120
Fault 12	120	60

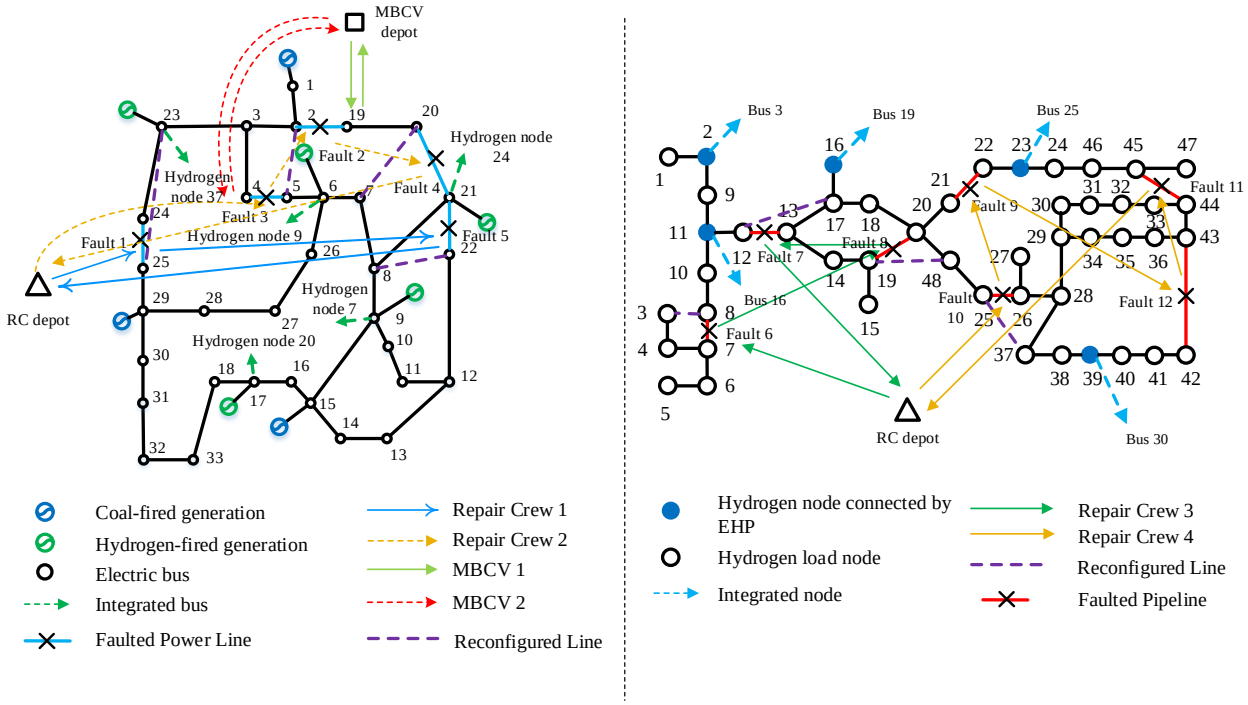

Fig. 4 RC and MBCV routes in the 33-bus-48-node IPHDS

In addition, Fig. 5 shows the hydrogen flows in the pipelines 2-9, 7-8 and 8-10. Different from the power flow in the power system, when the hydrogen network topology changes, the hydrogen flow cannot change immediately, but changes dynamically. For instance, after the pipeline 7-8 is damaged at the 0-th minute, the hydrogen flow in the pipeline 7-8 will remain 0, and the hydrogen loads at nodes 3, 4, 5, 6, and 7 will be shed until the fault is repaired at the 110-th minute. However, the hydrogen flow in the pipeline 2-9 cannot decrease immediately, and the excess hydrogen will become to line pack restoration in the pipelines, resulting in a temporary increase in the hydrogen flow of the pipeline 8-10. When the pipeline 7-8 is repaired, the hydrogen flows in these pipelines begin to gradually increase to support the restored hydrogen loads at nodes 3, 4, 5, 6, and 7, and will reach the steady -state values after the 400-th minute.

To investigate the influence of RCs, MBCVs, the dynamic hydrogen flow, and transportation states in the IPHDS restoration, we compare the restoration time and restored weighted loads in five cases:

Case 1: no RCs and MBCVs;

Case 2: 4 RCs and 2 MBCVs;

Case 3: 4 RCs and 2 MBCVs with the consideration of the dynamic hydrogen flow model;

Case 4: 4 RCs and 2 MBCVs with the consideration of the transportation state;

Case 5: 4 RCs and 2MBCVs with the consideration of the dynamic hydrogen flow and the transportation state.

Fig. 6 depicts the restored weighted loads at different time periods in these five cases. Firstly, during the given 550 minutes, the weighted load is only restored from 4.21 p.u. to 5.36 p.u. in Case 1. In contrast, the weighted load has increased to the normal state (12 p.u.) at the 480-th minute with the help of RCs and MBCVs in Case 2, which is more than 7.7 times faster than the restoration strategy in Case 1. Secondly, when the dynamic hydrogen flow model is applied to the IPHDS, the weighted load restoration will lag behind the network repairing and reconfiguration in nearly 60 minutes since the hydrogen flow cannot be changed instantaneously with the load demand. Therefore, the total weighted restored load in Case 3 is 3.7%-22.1% lower than

This article has been accepted for publication in a future issue of this journal, but has not been fully edited. Content may change prior to final publication. Citation information: DOI 10.1109/TIA.2021.3117926, IEEE Transactions on Industry Applications

that in Case 2 at each time period. Thirdly, if the transportation states (i.e., the traffic congestion) are considered in the restoration process, the repair sequence of the faulted power branches in Case 4 will be different. Compared with the restoration process in Case 2, although the weighted load restoration in Case 4 is 60 minutes slower in the first 200 minutes, the total restoration time in Case 4 is over 40 minutes less than that in Case 2. Finally, the dynamic hydrogen flow model and transportation states are both considered in Case 5, in which the traffic congestion and the dynamic hydrogen flow will both influence the restoration time. Before the 330-th minute, the total weighted restored load in Case 4 is 6%-33.9% lower than that in Case 2 at each time period. After the 330-th minute, the total weighted restored load in Case 5 is only 5% lower than that in Case 2 at each time period, and the total restoration time in Case 5 is 70 minutes longer than that in Case 2.

In the hydrogen system, RCs will also be dispatched to repair the fault pipelines closer to the RC depot (i.e., Fault 6 and Fault 10) first. Once Fault 6 and Fault 10 are recovered, the two islands in the hydrogen system will be reconnected and the corresponding hydrogen loads are picked up. Next, Fault 8 and Fault 7 will be repaired by RC3 in sequence, and Fault 9, Fault 12 and Fault 11 will be repaired by RC4 in sequence. Note that RC3 is dispatched to Fault 8 rather than Fault 7 after repairing Fault 6. It is because although the distance from Fault 6 to Fault 7 is shorter than that to Fault 8, the travel time from Fault 6 to Fault 7 is still longer than that to Fault 8 due to the traffic congestion. Similarly, RC4 is dispatched to Fault 12, rather than Fault 11 after repairing Fault 10.

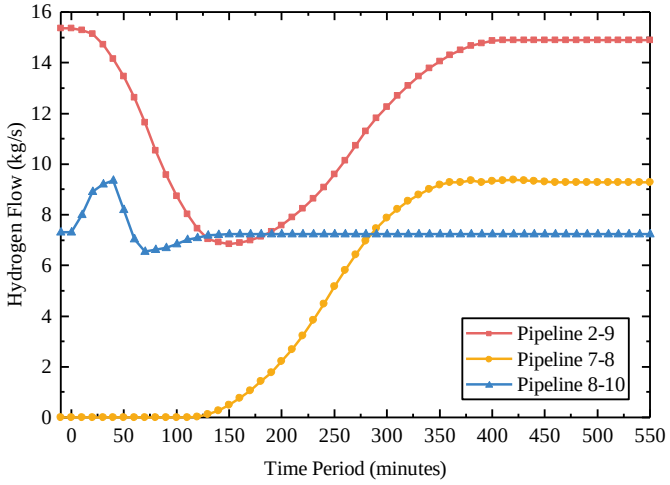

Fig. 5 Hydrogen flow in classic pipelines

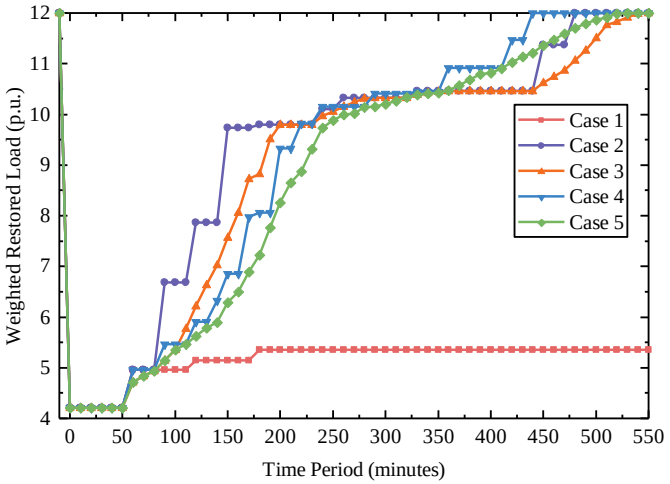

Fig. 6 Restored weighted loads in the 33-bus-48-node IPHDS

2) IPHDS integrated by a 144-bus distribution system and three hydrogen systems

In this part, a practical IPHDS with a 144-bus power distribution system and two hydrogen systems containing 85 nodes is derived from a region in China to further test the proposed MPRM model. The topologies for the 144-bus power distribution system and the hydrogen systems are shown in Fig. 7 and Fig. 8, respectively. There are 25 coal-fired generators with slow ramp rates; 6 hydrogen-fired generators, which can ramp up from the minimum to the maximum within 1 hour. The hydrogen system contains 85 hydrogen nodes that can be divided into 3 different small-scale hydrogen systems integrated with the power distribution system. In the hydrogen systems, there are 9 EHPs connecting with the power system. The capacity of each generator and EHPs is detailed in [48]. Besides, we also prioritize all power and hydrogen loads into five levels, demonstrating the load priority in [48]. The cascaded outages of 53 power branches and 25 pipelines are presented by red dashed lines in Fig. Fig. 7 and Fig. 8, which account for 31.5% of the total number of power branches and pipelines.

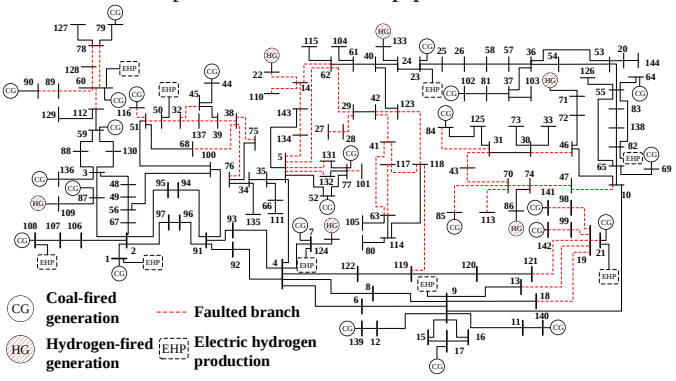

Fig. 7 Topology of 144-bus power distribution system

This article has been accepted for publication in a future issue of this journal, but has not been fully edited. Content may change prior to final publication. Citation information: DOI 10.1109/TIA.2021.3117926, IEEE Transactions on Industry Applications

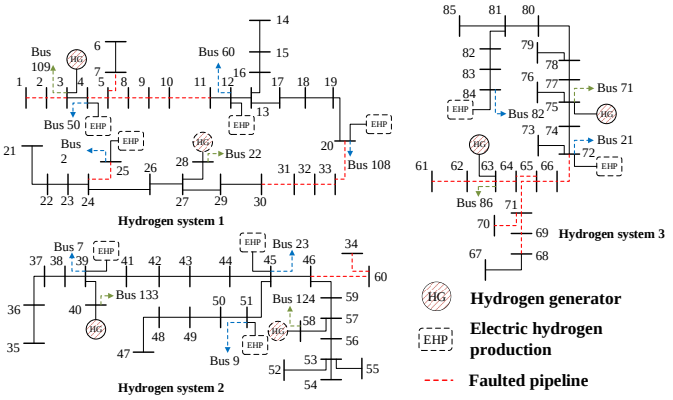

Fig. 8 Topology of the hydrogen systems

In this case, we assume that there are 5 RCs in the 144-bus power system, 3 RCs in the hydrogen systems and 5 different MBCVs in the IPHDS.

To investigate the influence of the dynamic hydrogen flow and transportation states on the IPHDS restoration, two different models are set up to compare with the proposed transportation state and dynamic hydrogen flow (MPRM): the restoration model only considering transportation state (RMTS), and the restoration model only considering dynamic hydrogen flow (RMDH). We sequentially compare the restoration time, restored weighted loads, the collaborative dispatch results of RCs and MBCVs, and the computational time for these three models.

Fig. 9 depicts the Gantt chart of the routes about two typical RCs deployed in the power system and the hydrogen system, and one MBCV in these three models. RC 1 is deployed in the power system, while RC 2 is deployed in the hydrogen system. The Gantt chart detailed the travel routes and repair tasks for the RCs and MBCV, where the scheduling orders are also shown in the Gantt chart. Based on the Gantt chart, the dynamic changes of transportation state and hydrogen flow can influence the RC and MBCV dispatch results in two aspects. Take RC 1 in the power system for an example. This RC will sequentially repair the branches 78-128, 128-60, 78-60, 89-60, 89-90, 60-112, 51-116, 50-51, 32-50, 32-137, 78-128, and 128-60. On the one hand, since the transportation state keeps changing, the time for RC 1 to complete all repair tasks in MPRM is 690 minutes, which is 80 minutes longer than those in RMTS and RMDH. On the other hand, the scheduling orders for RC 1 in three models were different from each other. Compared with the RC 1 routes in RMDH, the RC 1 in MPRM preferred to repair branches 51-116, 50-51, and 32-50 at first rather than branches 128-60, 89-60, and 89-90. The main reason is that there is a severe blockage in the path from branch 78-60 to branches 128-60, 89-60, and 89-90 at the beginning of the repair tasks. If RC 1 first repaired branches 128-60, 89-60, and 89-90, the total repair and travel time would be 240 minutes, while the total repair and travel time for RC 1 to repair branches 51-116, 50-51, and 32-50 was 210 minutes. To balance the repair time and travel time, RC 1 would first repair the branches with a relatively lower priority. As for RMTS and RMDH, the difference between scheduling orders of RC 1 in these two models indicates that the dynamic hydrogen flow will certainly influence the dispatch results. Since the hydrogen flow changes relatively slower than the power flow, the branches connected to the EHPs and hydrogen generators would require an earlier restoration. Thus, RC 1 preferred to repair branches 60-112 and 50-51 which are relatively connected with two EHPs.

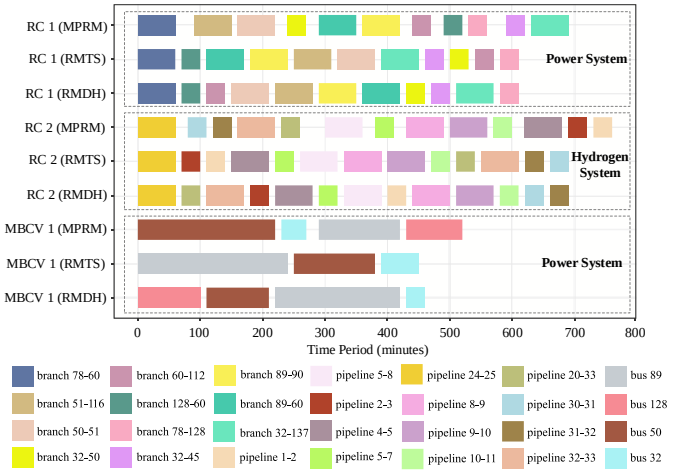

Fig. 9 Gantt chart of two typical RCs and one MBCV in three models

Furthermore, to illustrate the efficiency of the proposed model, the computational time for these three models is also investigated in this part, and three models are conducted by GUROBI on a computer with qua-core, 2.4 GHz CPU and 4 GB memory. Table III shows the computational time for three models, where we also simulate different outage scales by increasing faulted power branches and pipelines in the system, and compare the efficiency of the different models. The proposed MPRM takes into account both dynamic hydrogen flow model and transportation state, resulting in the longest computational time among these three models. RMDH considers the model of dynamic hydrogen flow which introduces the difference equations with numerous auxiliary variables into the restoration model. Thus, the computational time for RMDH is longer than that for RMTS. Generally, the computational time for MPRM is 18.1%-37.2% longer than that for RMTS and is 5.96%-23.9% longer than that for RMDH. With the increase in the number of faulted lines and expansion of the outage scale, the computational time of these three models gradually increases. When the number of faulted lines is doubled, the computational time will increase more than twice.

TABLE III COMPUTATIONAL TIME IN THREE MODELS

Number of faulted lines	Computational time (second)		
	MPRM	RMTS	RMDH
60	850.2	619.6	703.2
70	913.7	731.4	862.3
78	1127.5	955.3	1044.1
85	1594.4	1067.2	1198.3
95	103.2	1210.5	1322.3
100	1747.3	1302.5	1410.7
110	2011.3	1573.3	1655.3
120	2401.1	1902.1	2111.8

V. CONCLUSION

This paper proposed a multi-period restoration model for an integrated power and hydrogen distribution system with RCs, MBCVs, dynamic hydrogen flow, and transportation states. Once the outage happens, the network reconfiguration will be

first applied to avoid islanding. Then, RCs will be quickly dispatched to repair faulted lines under the consideration of the transportation state. MBCVs will also be dispatched to cooperate with RCs and support critical loads, which are located in islands. Numerical results showed that the hydrogen flow and hydrogen load restoration will be slightly lagging behind the pipeline repair and reconfiguration. Moreover, transportation states will influence the RC repair orders and routes. Therefore, considering dynamic hydrogen flow model and the transportation states, the restoration strategy will be much more realistic and viable, although the restoration time will be a little longer. Certainly, the computational time for the proposed model is longer than the model without the dynamic hydrogen flow.

REFERENCES

[1] Z. Bie, Y. Lin, G. Li, and F. Li, "Battling the Extreme: A Study on the Power System Resilience," *Proc. IEEE*, vol. 105, no. 7, pp. 1253-1266, 2017.

[2] T. Ding, M. Qu, Z. Wang, B. Chen, C. Chen, and M. Shahidehpour, "Power System Resilience Enhancement in Typhoons Using A Three-Stage Day-Ahead Unit Commitment," *IEEE Trans. Smart Grid*, Early Access, 2020.

[3] Y. Wang, C. Chen, J. Wang, and R. Baldick, "Research on Resilience of Power Systems Under Natural Disasters—A Review," *IEEE Trans. Power Syst.*, vol. 31, no. 2, pp. 1604-1613, 2016.

[4] P. Hoffman and W. Bryan, "Comparing the Impacts of Northeast Hurricanes on Energy Infrastructure," U.S. Department of Energy, Washington DC, USA 2013.

[5] Executive Office of the President, Economic Benefits of Increasing Electric Grid Resilience to Weather Outages, Tech. Rep., 2013.

[6] Z. Li, M. Shahidehpour, F. Aminifar, A. Alabdulwahab, and Y. Al-Turki, "Networked Microgrids for Enhancing the Power System Resilience," *Proc. IEEE*, vol. 105, no. 7, pp. 1289-1310, 2017.

[7] W. Yuan, J. Wang, F. Qiu, C. Chen, C. Kang, and B. Zeng, "Robust Optimization-Based Resilient Distribution Network Planning Against Natural Disasters," *IEEE Trans. Smart Grid*, vol. 7, no. 6, pp. 2817-2826, 2016.

[8] X. Wang, Z. Li, M. Shahidehpour, and C. Jiang, "Robust Line Hardening Strategies for Improving the Resilience of Distribution Systems With Variable Renewable Resources," *IEEE Trans. Sustain. Energy*, vol. 10, no. 1, pp. 386-395, 2019.

[9] N. L. Dehghani, A. B. Jeddi and A. Shafieezadeh, "Intelligent hurricane resilience enhancement of power distribution systems via deep reinforcement learning," *Appl. Energy*, vol. 285, p. 116355, 2021.

[10] B. Chen, C. Chen, J. Wang, K. L. Butler-Purry, and A. I. U. S. Argonne National Lab. ANL, "Sequential Service Restoration for Unbalanced Distribution Systems and Microgrids," *IEEE Trans. Power Syst.*, vol. 33, no. 2, pp. 1507-1520, 2018.

[11] F. Shen, Q. Wu, J. Zhao, W. Wei, N. D. Hatziargyriou, and F. Liu, "Distributed Risk-Limiting Load Restoration in Unbalanced Distribution Systems With Networked Microgrids," *IEEE Trans. Smart Grid*, vol. 11, no. 6, pp. 4574-4586, 2020.

[12] T. Ding, Y. Lin, G. Li and Z. Bie, "A New Model for Resilient Distribution Systems by Microgrids Formation," IEEE Trans. Power Syst., vol. 32, no. 5, pp. 4145-4147, Sept. 2017.

[13] T. Ding, Y. Lin, Z. Bie, and C. Chen, "A resilient microgrid formation strategy for load restoration considering master-slave distributed generators and topology reconfiguration," *Appl. Energy*, vol. 199, pp. 205-216, 2017.

[14] Y. Lin and Z. Bie, "Tri-level optimal hardening plan for a resilient distribution system considering reconfiguration and DG islanding," *Appl. Energy*, vol. 210, pp. 1266-1279, 2018.

[15] J. Liu, Y. Yu and C. Qin, "Unified two-stage reconfiguration method for resilience enhancement of distribution systems," *IET Gener. Transm. Distrib.*, vol. 13, no. 9, pp. 1734-1745, 2019.

[16] J. Xu, T. Zhang, Y. Du, W. Zhang, T. Yang, and J. Qiu, "Islanding and dynamic reconfiguration for resilience enhancement of active distribution systems," *Electr. Pow. Syst. Res.*, vol. 189, p. 106749, 2020.

[17] S. Lei, C. Chen, Y. Song, and Y. Hou, "Radiality Constraints for Resilient Reconfiguration of Distribution Systems: Formulation and Application to Microgrid Formation," *IEEE Trans. Smart Grid*, vol. 11, no. 5, pp. 3944-3956, 2020.

[18] Q. Shi, F. Li, M. Olama, J. Dong, Y. Xue, M. Starke, C. Winstead, and T. Kuruganti, "Network reconfiguration and distributed energy resource scheduling for improved distribution system resilience," *Int. J. Electr. Power Energy Syst.*, vol. 124, p. 106355, 2021.

[19] G. Glenk and S. Reichelstein, "Economics of converting renewable power to hydrogen," *Nat. Energy*, vol. 4, no. 3, pp. 216-222, 2019.

[20] G. Pan, W. Gu, Y. Lu, H. Qiu, S. Lu, and S. Yao, "Optimal Planning for Electricity-Hydrogen Integrated Energy System Considering Power to Hydrogen and Heat and Seasonal Storage," *IEEE Trans. Sustain. Energy*, vol. 11, no. 4, pp. 2662-2676, 2020.

[21] M. Shahidehpour, X. Wang, C. Shao, X. Wang, Q. Zhou, and C. J. Feng, "Optimal Stochastic Operation of Integrated Electric Power and Renewable Energy with Vehicle-Based Hydrogen Energy System," *IEEE Trans. Power Syst.*, Early Access, 2021.

[22] Y. Tao, J. Qiu, S. Lai, and J. Zhao, "Integrated Electricity and Hydrogen Energy Sharing in Coupled Energy Systems," *IEEE Trans. Smart Grid*, Early Access, 2020.

[23] J. Li, J. Lin, Y. Song, X. Xing, and C. Fu, "Operation Optimization of Power to Hydrogen and Heat (P2HH) in ADN Coordinated With the District Heating Network," *IEEE Trans. on Sustain. Energy*, vol. 10, no. 4, pp. 1672-1683, 2019.

[24] M. Ban, J. Yu, M. Shahidehpour, and Y. Yao, "Integration of power-to-hydrogen in day-ahead security-constrained unit commitment with high wind penetration," *J. Mod. Power Syst. Clean Energy*, vol. 5, no. 3, pp. 337-349, 2017.

[25] T. Yun, W. Zedi, L. Yan, M. Qian, H. Qian, L. Shubin, G. L. E. P. State, D. A. C. C. Power, U. O. T. Shenyang, and G. E. I. M. State, "Multi energy storage system model based on electricity heat and hydrogen coordinated optimization for power grid flexibility," *CSEE J. Power Energy Syst.*, vol. 5, no. 2, pp. 266-274, 2019.

[26] T. Ding, Y. Hu and Z. Bie, "Multi-Stage Stochastic Programming With Nonanticipativity Constraints for Expansion of Combined Power and Natural Gas Systems," IEEE Trans. Power Syst., vol. 33, no. 1, pp. 317-328, Jan. 2018.

[27] Z. Zhang, T. Ding, Q. Zhou, et al., "A review of technologies and applications on versatile energy storage systems", Renewable & Sustainable Energy Reviews, doi:10.1016/j.rser.2021.111263.

[28] Z. Zeng, T. Ding, Y. Xu, Y. Yang and Z. Dong, "Reliability Evaluation for Integrated Power-Gas Systems With Power-to-Gas and Gas Storages," IEEE Trans. Power Syst. vol. 35, no. 1, pp. 571-583, Jan. 2020.

[29] S. Lei, C. Chen, Y. Li, and Y. Hou, "Resilient Disaster Recovery Logistics of Distribution Systems: Co-Optimize Service Restoration With Repair Crew and Mobile Power Source Dispatch," *IEEE Trans. Smart Grid*, vol. 10, no. 6, pp. 6187-6202, 2019.

[30] B. Cen, Z. Ye, C. Chen, J. Wang, T. Ding, Z. Bie, and A. I. U. S. Argonne National Lab. ANL, "Toward a Synthetic Model for Distribution System Restoration and Crew Dispatch," *IEEE Trans. Power Syst.*, vol. 34, no. 3, pp. 2228-2239, 2019.

[31] S. Lei, J. Wang, C. Chen, Y. Hou, and A. I. U. S. Argonne National Lab. ANL, "Mobile Emergency Generator Pre-Positioning and Real-Time Allocation for Resilient Response to Natural Disasters," *IEEE Trans. Smart Grid*, vol. 9, no. 3, pp. 2030-2041, 2018.

[32] T. Paolo and V. Daniele, *The vehicle routing problem*: Society for Industrial and Applied Mathematics, 2002.

[33] Y. Lin, B. Chen, J. Wang, and Z. Bie, "A Combined Repair Crew Dispatch Problem for Resilient Electric and Natural Gas System Considering Reconfiguration and DG Islanding," *IEEE Trans. Power Syst.*, vol. 34, no. 4, pp. 2755-2767, 2019.

[34] Y. Xu, Y. Wang, J. He, M. Su, and P. Ni, "Resilience-Oriented Distribution System Restoration Considering Mobile Emergency Resource Dispatch in Transportation System," *IEEE Access*, vol. 7, pp. 73899-73912, 2019.

[35] A. Arif, Z. Wang, J. Wang, and C. Chen, "Power Distribution System Outage Management With Co-Optimization of Repairs, Reconfiguration, and DG Dispatch," *IEEE Trans. Smart Grid*, vol. 9, no. 5, pp. 4109-4118, 2018.

[36] G. Zhang, F. Zhang, X. Zhang, Z. Wang, K. Meng, and Z. Y. Dong, "Mobile Emergency Generator Planning in Resilient Distribution Systems: A

Three-Stage Stochastic Model With Nonanticipativity Constraints," *IEEE Trans. Smart Grid*, vol. 11, no. 6, pp. 4847-4859, 2020.
[37] T. Ding, Z. Wang, W. Jia, B. Chen, C. Chen, and M. Shahidehpour, "Multiperiod Distribution System Restoration With Routing Repair Crews, Mobile Electric Vehicles, and Soft-Open-Point Networked Microgrids," *IEEE Trans. Smart Grid*, vol. 11, no. 6, pp. 4795-4808, 2020.
[38] T. Ding, S. Liu, W. Yuan, Z. Bie and B. Zeng, "A Two-Stage Robust Reactive Power Optimization Considering Uncertain Wind Power Integration in Active Distribution Networks," IEEE Trans. Sustainable Enery., vol. 7, no. 1, pp. 301-311, Jan. 2016.
[39] T. Ding, C. Li, Y. Yang, J. Jiang, Z. Bie and F. Blaabjerg, "A Two-Stage Robust Optimization for Centralized-Optimal Dispatch of Photovoltaic Inverters in Active Distribution Networks," IEEE Trans. Sustainable Enery., vol. 8, no. 2, pp. 744-754, April 2017.
[40] H. Zang, L. Cheng, T. Ding, et al., "Day-ahead photovoltaic power forecasting approach based on deep convolutional neural networks and meta learning", Int. J. Electr. Power Energy Syst., vol. 118, pp. 105790, Jun. 2020.
[41] H. Zang, L. Cheng, T. Ding, et al., "Estimation and validation of daily global solar radiation by day of the year-based models for different climates in China", Renewable Energy, vol. 135, pp. 984-1003, May 2019.
[42] R. Teixeira Pinto, M. Aragues-Penalba, O. Gomis-Bellmunt, and A. Sumper, "Optimal Operation of DC Networks to Support Power System Outage Management," *IEEE Trans. Smart Grid*, vol. 7, no. 6, pp. 2953-2961, 2016.
[43] T. Ding, R. Bo, W. Gu, and H. Sun, "Big-M Based MIQP Method for Economic Dispatch with Disjoint Prohibited Zones," *IEEE Trans. Power Syst.*, vol. 29, no. 2, pp. 976–977, 2014.
[44] J. Fang, Q. Zeng, X. Ai, Z. Chen, and J. Wen, "Dynamic Optimal Energy Flow in the Integrated Natural Gas and Electrical Power Systems," *IEEE Trans. on Sustain. Energy*, vol. 9, no. 1, pp. 188-198, 2018.
[45] A. R. Gourlay and J. L. Morris, "Finite-Difference Methods for Nonlinear Hyperbolic Systems," *Math. Comput.*, vol. 22, no. 101, pp. 28-39, 1968.
[46] M. Behbahani-Nejad and Y Shekari, "Reduced order modeling of natural gas transient flow in pipelines," *Int. J. Eng. Appl. Sci.*, vol. 7, no. 5, pp. 148-152, 2008.
[47] A. D. Woldeyohannes and M. A. A. Majid, "Simulation model for natural gas transmission pipeline network system," *Simul. Model. Pract. Theory*, vol. 19, no. 1, pp. 196-212, 2011.
[48] https://github.com/ZekaiWang-XJTU/data-of-33-bus-distribution-network

Zekai Wang (S'20) received the B.S. degree from the School of Electrical Engineering, Xi'an Jiaotong University, Xi'an, China, in 2018. He is currently working toward the M.S. degree at Xi'an Jiaotong University. His major research interests include power system optimization and resilience.

Tao Ding (SM'19) received the B.S.E.E. and M.S.E.E. degrees from Southeast University, Nanjing, China, in 2009 and 2012, respectively, and the Ph.D. degree from Tsinghua University, Beijing, China, in 2015. During 2013 and 2014, he was a Visiting Scholar in the Department of Electrical Engineering and Computer Science, University of Tennessee, Knoxville, TN, USA. He is currently an Associate Professor in the State Key Laboratory of Electrical Insulation and Power Equipment, the School of Electrical Engineering, Xi'an Jiaotong University. His current research interests include electricity markets, power system economics and optimization methods, and power system planning and reliability evaluation. He has published more than 60 technical papers and authored by "Springer Theses" recognizing outstanding Ph.D. research around the world and across the physical sciences—*Power System Operation with Large Scale Stochastic Wind Power Integration*. He received the excellent master and doctoral dissertation from Southeast University and Tsinghua University, respectively, and Outstanding Graduate Award of Beijing City. Dr. Ding is an editor of IEEE Transactions on Power Systems, IEEE Power Engineering Letters, IEEE Systems Journal, IET Generation Transmission & Distribution and CSEE JPES.

Weihao Jia (S'20) received the B.S. degree from the School of Electrical Engineering, Xi'an Jiaotong University, Xi'an, China, in 2020. He is currently working toward the M.S. degree at Xi'an Jiaotong University. His major research interests include power system optimization and renewable energy integration.

Can Huang (S'13-M'16-SM'18) received the B.S.E.E degree from Hohai University, Nanjing, China, in 2008, the M.S.E.E. degree from Southeast University, Nanjing, China, in 2011, and the Ph.D. degree in Electrical Engineering from the University of Tennessee, Knoxville, TN, USA, in 2016. Now he is a Research Staff with Lawrence Livermore National Laboratory, Livermore, CA, USA. His current research interests include smart sensors, data analytics, and machine learning for energy and power systems, cyber-physical systems, and Internet of Things.

João P. S. Catalão (Senior Member, IEEE) received the M.Sc. degree from the Instituto Superior Técnico (IST), Lisbon, Portugal, in 2003, and the Ph.D. degree and Habilitation for Full Professor ("Agregação") from the University of Beira Interior (UBI), Covilha, Portugal, in 2007 and 2013, respectively. Currently, he is a Professor at the Faculty of Engineering of the University of Porto (FEUP), Porto, Portugal, and Research Coordinator at INESC TEC. He was also appointed as Visiting Professor by North China Electric Power University (NCEPU), Beijing, China. His research interests include power system operations and planning, distributed renewable generation, power system economics and electricity markets, demand response and smart grid.